

Optimization hardness as transient chaos in an analog approach to constraint satisfaction*

Mária Ercsey-Ravasz^{1,3†} and Zoltán Toroczkai^{1,2‡}

¹ Department of Physics, University of Notre Dame, Notre Dame, IN, 46556 USA and Interdisciplinary Center for Network Science and Applications (iCeNSA)

² Departments of Computer Science and Engineering, University of Notre Dame, Notre Dame, IN, 46556 USA

³ Faculty of Physics, Babes-Bolyai University, Cluj-Napoca, Romania

November 27, 2024

Abstract

Boolean satisfiability [1] (k -SAT) is one of the most studied optimization problems, as an efficient (that is, polynomial-time) solution to k -SAT (for $k \geq 3$) implies efficient solutions to a large number of hard optimization problems [2, 3]. Here we propose a mapping of k -SAT into a deterministic continuous-time dynamical system with a unique correspondence between its attractors and the k -SAT solution clusters. We show that beyond a constraint density threshold, the analog trajectories become transiently chaotic [4, 5, 6, 7], and the boundaries between the basins of attraction [8] of the solution clusters become fractal [7, 8, 9], signaling the appearance of optimization hardness [10]. Analytical arguments and simulations indicate that the system always finds solutions for satisfiable formulae even in the frozen regimes of random 3-SAT [11] and of locked occupation problems [12] (considered among the hardest algorithmic benchmarks); a property partly due to the systems hyperbolic [4, 13] character. The system finds solutions in polynomial continuous-time, however, at the expense of exponential fluctuations in its energy function.

*The article appeared in *Nature Physics* **7**, 966 (2011)

†E-mail: ercsey.ravasz@phys.ubbcluj.ro

‡E-mail: toro@nd.edu

Boolean satisfiability [1] (k -SAT, $k \geq 3$) is the quintessential constraint satisfaction problem, lying at the basis of many decision, scheduling, error-correction and bio-computational applications. k -SAT is in NP, that is its solutions are efficiently (polynomial time) checkable, but no efficient (polynomial time) algorithms are known to compute those solutions [2]. If such algorithms would be found for k -SAT, all NP problems would be efficiently computable, since k -SAT is NP-complete [2, 3].

In k -SAT there are given N Boolean variables $\{x_1, \dots, x_N\}$, $x_i \in \{0, 1\}$ and M clauses (constraints), each clause being the disjunction (OR, denoted as \vee) of k variables or their negation (\bar{x}). One has to find an assignment of the variables such that all clauses (called collectively as a formula) are satisfied (TRUE = 1). When the number of constraints is small, it is easy to find solutions, while for too many constraints it is easy to decide that the formula is unsatisfiable (UNSAT). Deciding satisfiability, in the 'intermediate range', however, can be very hard: the worst-case complexity of all known algorithms for k -SAT is exponential in N .

Inspired by the mechanisms of information processing in biological systems, analog computing received increasing interest from both theoretical [14, 15, 16] and engineering communities [17, 18, 19, 20, 21]. Although the theoretical possibility of efficient computation via chaotic dynamical systems has been shown previously [15], nonlinear dynamical systems theory has not been exploited for NP-complete problems in spite of the fact that, as shown by Gu et al. [19], Nagamatu et al. [20] and Wah et al. [21], k -SAT can be formulated as a continuous global optimization problem [19], and even cast as an analog dynamical system [20, 21].

Here we present a novel continuous-time dynamical system for k -SAT, with a dynamics that is rather different from previous approaches. Let us introduce the continuous variables [19] $s_i \in [-1, 1]$, such that $s_i = -1$ if the i -th variable (x_i) is FALSE and $s_i = 1$ if it is TRUE. We define $c_{mi} = 1$ for the direct form (x_i), $c_{mi} = -1$ for the negated form (\bar{x}_i), and $c_{mi} = 0$ for the absence of the i -th variable from clause m . Defining the constraint function $K_m(\mathbf{s}) \equiv 2^{-k} \prod_{i=1}^N (1 - c_{mi}s_i)$ corresponding to clause m , we have $K_m \in [0, 1]$ and $K_m = 0$ if and only if clause m is satisfied. The goal would be to find a solution \mathbf{s}^* with $s_i^* \in \{-1, 1\}$ to $E(\mathbf{s}^*) = 0$, where E is the energy function $E(\mathbf{s}) = \sum_{m=1}^M K_m(\mathbf{s})^2$. If such \mathbf{s}^* exists, it will be a global minimum for E and a solution to the k -SAT problem. However, finding \mathbf{s}^* by a direct minimization of $E(\mathbf{s})$ will typically fail due to non-solution attractors trapping the search dynamics. In order to avoid such traps, here we define a modified energy function $V(\mathbf{s}, \mathbf{a}) = \sum_{m=1}^M a_m K_m(\mathbf{s})^2$, using auxiliary variables $a_m \in (0, \infty)$ similar to Lagrange multipliers [20, 21]. Let us denote by \mathcal{H}_N the continuous domain $[-1, 1]^N$. Its boundary is the N -hypercube $Q_N = \partial\mathcal{H}_N$ with vertex set $\mathcal{V}_N = \{-1, 1\}^N \subset Q_N$. The set of solutions for a given k -SAT formula, called solution space, occupies a subset of \mathcal{V}_N . *Solution clusters* are formed by solutions that can be connected via *single-variable* flips, always staying within satisfying assignments [22]. Clearly, $V \geq 0$ in $\Omega \equiv \mathcal{H}_N \times (0, \infty)^M$, and $V(\mathbf{s}, \mathbf{a}) = 0$ within \mathcal{V}_N if and only if $\mathbf{s} = \mathbf{s}^* \in \mathcal{V}_N$ is a k -SAT solution, for any $\mathbf{a} \in (0, \infty)^M$. We now introduce a *continuous-time dynamical system* on Ω through:

$$\frac{ds_i}{dt} = (-\nabla_{\mathbf{s}} V(\mathbf{s}, \mathbf{a}))_i = \sum_{m=1}^M 2a_m c_{mi} K_{mi}(\mathbf{s}) K_m(\mathbf{s}), \quad i = 1, \dots, N, \quad (1)$$

$$\frac{da_m}{dt} = a_m K_m(\mathbf{s}), \quad m = 1, \dots, M, \quad (2)$$

where ∇_s is the gradient operator with respect to s , and $K_{mi} = K_m/(1 - c_{mi}s_i)$. The initial conditions for s are arbitrary $s(0) \in \mathcal{H}_N$, however, for a they have to be strictly positive, $a_m(0) > 0$ (e.g., $a_m(0) = 1$). The k -SAT solutions $s^* \in \mathcal{V}_N$ are fixed points of (1-2), for any $a \in (0, \infty)^M$. The k -SAT solution clusters are spanning piecewise compact, connected sets in Q_N , and every point in them is a fixed point of (1-2) (Supplementary sect. A). System (1-2) has a number of key properties (see Supplementary Information). (i) The dynamics in s stays confined to \mathcal{H}_N . (ii) The k -SAT solutions $s^* \in \mathcal{V}_N$ are attractive fixed points of (1-2). In particular, every point s from the orthant of a k -SAT solution s^* with the property $|s|^2 \geq N - 1 + (k - 1)^2/(k + 1)^2$ is guaranteed to flow into the attractor corresponding to s^* . (iii) There are no limit cycles. (iv) For satisfiable formulae the only fixed point attractors of the dynamics are the global minima of V with $V = 0$. Note that in principle, the projection of the dynamics onto \mathcal{H}_N could be stuck in some point \bar{s} , while $da/dt \neq 0$ indefinitely. This does not happen here, as shown in Supplementary sect. E. Moreover, analytical arguments supported by simulations indicate that the trajectory will leave any domain that does not contain solutions, see the discussion in Supplementary sect. E1. Note, that the constraint functions (hence their satisfiability) depend directly only on the location of the trajectory in \mathcal{H}_N , $K_m = K_m(s)$, and not on the auxiliary variables. The dynamics in the a -space is simple expansion, and for this reason the features of the full phase space Ω lie within its projection onto \mathcal{H}_N . One can actually eliminate entirely the auxiliary variables from the equations by first solving (2) to give $a_m(t) = a_m(0) \exp\left(\int_0^t K_m(s(\tau))d\tau\right)$ then inserting it into (1).

Another fundamental feature of (1-2) is that it is *deterministic*: for a given formula f , any initial condition generates a unique trajectory, and any set from \mathcal{H}_N has a unique preimage arbitrarily back in time. Hence, the characteristics of the solution space are reflected in the properties of the invariant sets [7] of the dynamics (1-2) within the hypercube \mathcal{H}_N . The deterministic nature of (1-2) allows us to define basins of attractions of solution clusters by colouring every point in \mathcal{H}_N according to which cluster the trajectory flows to, if started from there. These basins fill \mathcal{H}_N up to a set of zero (Lebesgue) measure, which forms the basin boundary [7], from where the dynamics (by definition) cannot flow to any of the attractors. A k -SAT formula f can be represented as a hypergraph $\mathcal{G}(f)$ (or equivalently, a factor graph) in which nodes are variables and hyperedges are clauses connecting the nodes/variables in the clause. Pure literals are those that participate in one or more clauses but always in the same form (direct or negated); hence they can always be chosen such as to satisfy those clauses. The core of $\mathcal{G}(f)$ is the subgraph left after sequentially removing all the hyperedges having pure literals [23]. For simple formulae (such as those without a core), the dynamics of (1-2) is laminar flow and the basin boundaries form smooth, non-fractal sets (Fig. 1a,c and Fig. 2 top two rows). Adding more constraints $\mathcal{G}(f)$ develops a core, the spin equations (1) become mutually coupled, and the trajectories may become chaotic (Fig. 1b, Supplementary sect. F, Fig. 12) and the basin boundaries fractal [7, 8, 9] (Fig. 1d, Fig. 2, Fig. 8). Therefore, as the constraint density $\alpha = M/N$ is increased within predefined ensembles of formulae (random k -SAT, occupation problems, k -XORSAT, etc.) a sharp change to chaotic behaviour is expected at a *chaotic transition point* α_χ , where a *chaotic core* appears with non-zero statistical weight in the ensemble as $N \rightarrow \infty$. As an example, let us consider 3-XORSAT. In this case, due to its inherently linear nature, it is actually better to work directly with the parity check equations as constraints, instead of their CNF form. The chaotic core here is a small finite hypergraph, and

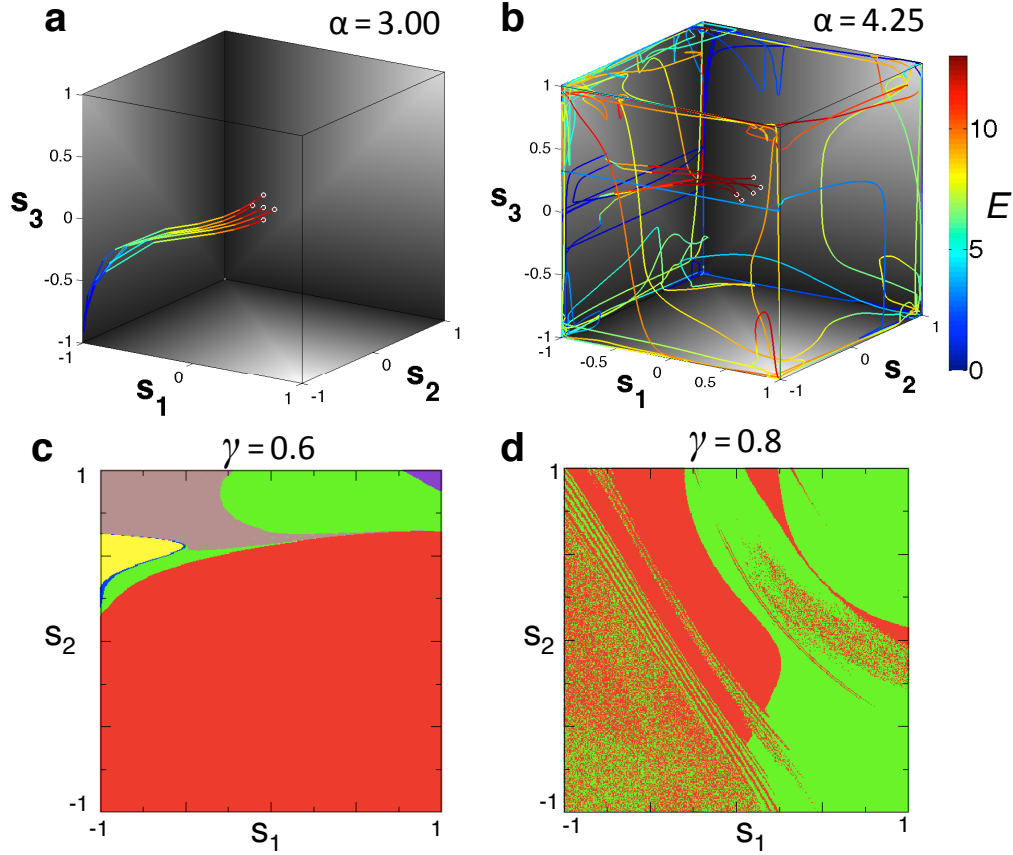


Figure 1: **Chaotic behaviour.** Five, closely started sample trajectories projected onto (s_1, s_2, s_3) a), for a 3-SAT formula with $N = 200$, $\alpha = 3$ and b) for a hard formula, $N = 200$, $\alpha = 4.25$. The colour indicates the energy E (colour bar) in a given point of the trajectory. While for easy formulae the trajectories exhibit laminar flow, for hard formulae they quickly become separated, showing a chaotic evolution. Taking a small 3-XORSAT instance with $N = 15$ (see Supplementary sect. G) we fix a random initial condition for all s_i , except s_1 and s_2 which are varied on a 400×400 grid and we colour each point according to the solution they flow to for c) $\gamma = 0.6$ (instance shown on Fig. 8e) and d) for $\gamma = 0.8$ (instance shown in Fig. 8f)).

thus α_χ coincides with the so-called dynamical transition point computed exactly by Mézard et al. [24] (see Supplementary sect. G and Fig. 8). Note, a core can be non-chaotic, and thus the existence of a core is only a *necessary* condition for the appearance of chaos and in general the two transitions might not coincide. Further increasing the number of constraints (within any formula ensemble) unsatisfiability appears at the threshold value $\alpha_s > \alpha_\chi$ beyond which almost all formulae are unsatisfiable (UNSAT regime)[11, 12, 22, 24, 25, 26, 27, 28]. The closer α is to α_s , the harder it is to find solutions, and beyond the so-called freezing transition point $\alpha_f < \alpha_s$ (called the frozen regime) all known algorithms take exponentially long times or simply fail to find solutions [11, 12]. A variable is frozen if it takes on the same value for all solutions within a cluster, and a cluster is frozen if an extensive number of its variables are frozen. In the frozen regime all clusters are frozen and they are also far apart ($\mathcal{O}(N)$ Hamming distance)[11, 12]. For random 3-SAT (clauses chosen uniformly at random for fixed α) $\alpha_s \cong 4.26$ [27], $\alpha_f \cong 4.25$ [28] and all known local search algorithms become exponential or fail beyond $\alpha = 4.21$ [29], while Survey Propagation [25] based algorithms fail beyond $\alpha = 4.25$ [28]. Since the frozen regime is very thin in random 3-SAT, Zdeborová and Mézard [12] have introduced the so-called locked occupation problems (LOPs). In LOPs all clusters are formed by exactly one solution, hence they are completely frozen and the frozen regime extends from the clustering (dynamical) transition point l_d to the satisfiability threshold l_s , and thus it is very wide [12]. An example LOP is random +1-in-3-SAT [12], made of constraints that have no negated variables and a constraint is satisfied only if exactly one of its variables is 1 (TRUE). In +1-in-3-SAT $l_d \cong 2.256$, $l_s \cong 2.368$, and beyond l_d all known algorithms have exponential search times or fail to find solutions (here $l = 3M/N$).

As chaos is present for satisfiable formulae, that is, when system (1-2) *has* attracting fixed points, it is necessarily of *transient* type. Transient chaos [4, 5, 6, 7] is ubiquitous in systems with many degrees of freedom such as fluid turbulence [30]. It appears as the result of homoclinic/heteroclinic intersections of the invariant manifolds of hyperbolic (unstable) fixed points of (1-2) lying within the basin boundary [7, 8, 9], leading to complex (fractal) foliations of the phase space (see Supplementary sect. F). We observed the prevalence of transient chaos in the whole region $\alpha_\chi < \alpha < \alpha_s$ for all the problem classes we studied. Interestingly, the velocity fluctuations of trajectories in the chaotic regime are qualitatively similar to those of fluid parcels in turbulent flows as shown in Supplementary sect. K. Our findings suggest that chaotic behaviour may be a generic feature of algorithms searching for solutions in hard optimization problems, corroborating the observations by Elser et al.[10] using a heuristic algorithm based on iterated maps.

In the following we show results on random 3-SAT and +1-in-3-SAT formulae in the frozen regime, however, the same conclusions hold for other ensembles that we tested. To investigate the complexity of computation by the flow (1-2), we monitored the fraction of problems $p(t)$ not solved by continuous time t , as function of N and α . Figs. 3a,c show that even in the frozen phase, the fraction of unsolved problems by time t decays exponentially with t , that is, by a law $p(t) = re^{-\lambda(N)t}$. The decay rate $\lambda(N)$ obeys $\lambda(N) = bN^{-\beta}$, with $\beta \simeq 1.6$ in both cases, see Fig. 3b,d. From these two equations, the continuous-time $t(p, N)$ needed to solve a fixed $(1 - p)$ th fraction of random formulae (or to miss solving p -th fraction of them) is:

$$t(p, N) = b^{-1}N^\beta \ln(r/p) \quad (3)$$

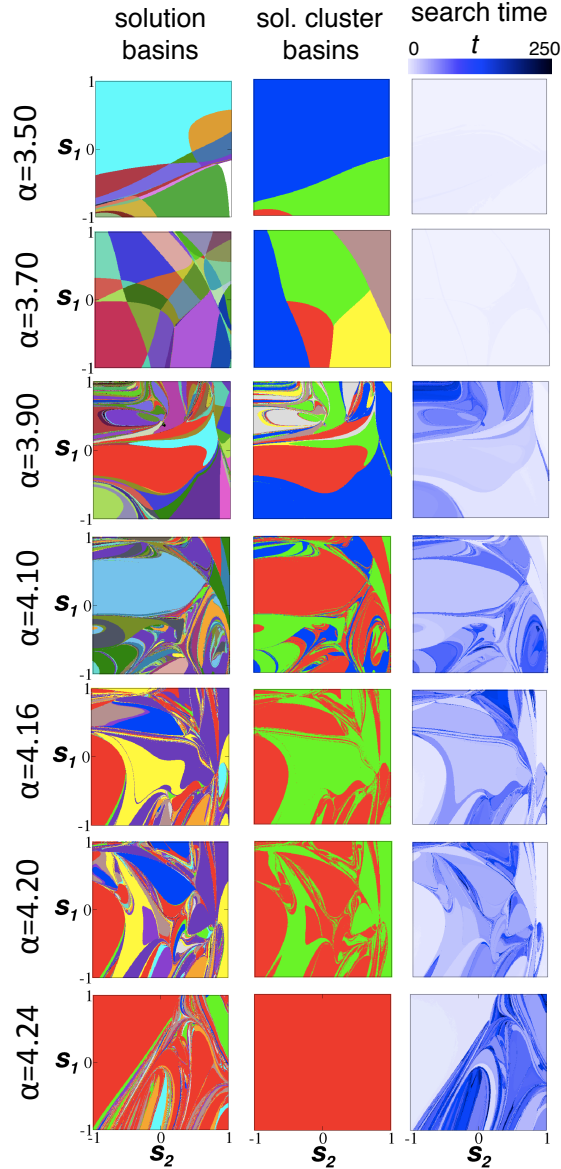


Figure 2: **Attractor basins.** For a random 3-SAT instance with $N = 50$ we vary α by successively adding new constraints. Fixing a random initial condition for s_i , $i \geq 3$, we vary only s_1 and s_2 on a 400×400 grid, and we colour each point according to the solution (first column) or solution cluster (second column) they flow to. Each colour in a given column represents a solution or solution cluster respectively, however colours between columns are independent. The third column represents the analog search time t needed to find a solution (see colour bar) starting from the corresponding grid point. Maps are presented for values of $\alpha = 3.5, 3.7, 3.9, 4.1, 4.16, 4.2, 4.24$. Easy formulae are characterized by smooth basin boundaries and small search times. Note that we only see the solutions (and clusters) that reveal themselves in the (s_1, s_2) plane, others might not be seen. For hard formulae the boundaries and the search time maps become fractal.

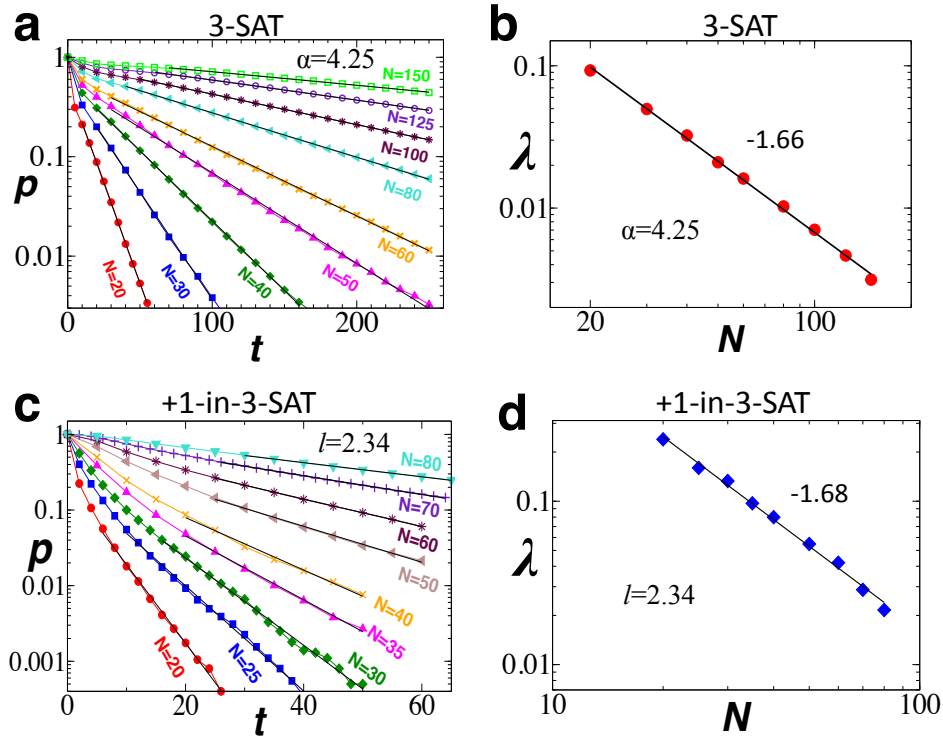


Figure 3: **Computational complexity properties.** a) The fraction of problems $p(t)$ not yet solved by continuous-time t for 3-SAT at $\alpha = 4.25$, for $N = 20, 30, 40, 50, 60, 80, 100, 125, 150$ (colours). Averages were done over 10^5 instances for each N . For each instance the dynamics was started from one random initial condition. Black continuous lines show the decay $p(t) = r \exp(-\lambda(N)t)$. b) The decay rate follows $\lambda(N) = bN^{-\beta}$, with $\beta \simeq 1.66$. c) The fraction of problems $p(t)$ unsolved by time t for +1-in-3-SAT at $l = 2.34$, for $N = 20, 25, 30, 35, 40, 50, 60, 70, 80$. For each instance the dynamics was started in parallel from 10 random initial conditions, averages were taken over 10^4 instances for each N . Black continuous lines show the same exponential decay as in a). d) The decay rate shows the same behaviour as in b) with exponent: $\beta \simeq 1.68$.

indicating that the continuous time (CT) needed to find solutions scales as a power-law with N . Eq. (3) also implies power-law scaling for almost all hard instances in the $N \rightarrow \infty$ limit (Supplementary sect. H). The *length* in \mathcal{H}_N of the corresponding continuous trajectories also scales as a power-law with N (Supplementary Fig. 11b, sect. J). However, note that this does not mean that the algorithm itself is a polynomial-cost algorithm, as the energy function V can have exponentially large fluctuations. As the numerical integration happens on a digital machine, it approximates the continuous trajectory with discrete points. Monitoring the fraction of formulae left unsolved as function of the number of discretization steps n_{step} in the frozen phase, we find exponential behaviour for $n_{step}(p, N)$ (Supplementary sects. I,J, Fig. 10). The difference between the continuous- and discrete-time complexities is due to the wildly fluctuating nature of the chaotic trajectories (see Fig. 1b and Methods) in the frozen phase. Compounding this, we also observe the appearance of the Wada property [7, 8] in the basin boundaries, Fig. 4. A fractal basin boundary has Wada property if its points are simultaneously on the boundary of at least three colours/basins. (An amusing method that creates such sets uses four Christmas ball ornaments[7].) Although the Wada property does not affect the true/mathematical analog trajectories, owing to numerical errors, it may switch the numerical trajectories between the basins. Since the clusters are far ($\mathcal{O}(N)$) apart, the switched trajectory will flow towards another cluster into a practically opposing region of \mathcal{H}_N until it may come close again to the basin boundary etc., partially randomizing the trajectory in \mathcal{H}_N .

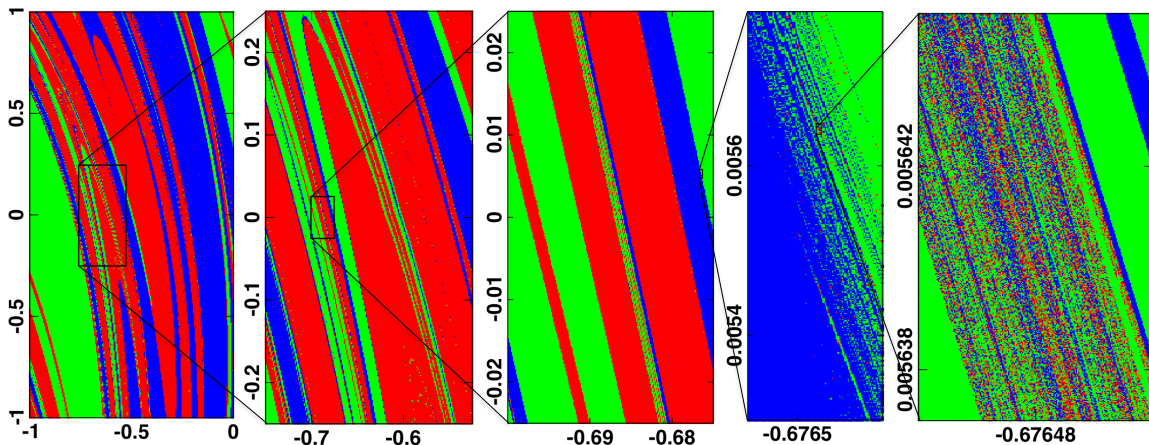


Figure 4: **Wada property.** Basin boundaries are shown for +1-in-3-SAT for an instance at $N = 30$ and $l = 2.28$. Fixing a random initial condition for all s_i , $i \geq 3$ we vary only s_1 and s_2 on a 200×400 grid and colour the points according to three different solutions they flow to. Successive magnifications illustrate the Wada property: the points on the basin boundaries are simultaneously on the boundary of all three basins implying that large enough magnifications will contain all three colours (although the blue-green boundary seems void of red in the third panel, panels four and five show that red is actually present).

We conjecture that the power-law scaling of the continuous search times (3) is due in part to a generic property of the dynamical system (1-2), namely that it is *hyperbolic* [4, 6, 13], or near-

hyperbolic. It has been shown that for hyperbolic systems the trajectories escape from regions far away from the attractors to the attractors at an *exponential rate*, for almost all initial conditions [4, 6, 13]. That is, the fraction of trajectories still searching for a solution after time t decays as $e^{-\kappa t}$ (Supplementary Fig. 13), where κ is the *escape rate*. Thus, κ^{-1} can be considered as a measure of hardness for a *given formula*. When taken over an ensemble at a given α , this property generates the exponential decay for $p(t)$ with an average escape rate λ .

The form of the energy function V incorporates the influence of all the clauses at all times, and in this sense the system (1-2) is a non-local search algorithm. As shown before, the auxiliary variables can be eliminated, however, they give a convenient interpretation of the dynamics. Namely, one can think of them as providing extra dimensions along which the trajectories escape from local wells, and their form (2) provides positive feedback that guarantees their escape. Clearly, these equations are not unique, and other forms based on the same principles may work just as well.

Methods

To simulate (1-2), we use a 5-th order adaptive Cash-Karp Runge-Kutta method with monitoring of local truncation error to ensure accuracy. In order to keep the numerical trajectory within a tube of small, preset thickness around the true analog trajectory in Ω (Supplementary Fig. 9), the RK algorithm occasionally performs an exponentially large number of discretization steps n_{step} . However, this only happens for hard formulae, when the analog trajectory has wild, chaotic fluctuations. For easy formulae both $p(t)$ and $p(n_{step})$ decay exponentially as shown in Supplementary Fig. 10a, inset.

Acknowledgments

We thank T. Tél and L. Lovász for valuable discussions and for a critical reading of the manuscript.

Author contributions

M.E.R. and Z.T. conceived and designed the research and contributed analysis tools equally. M.E.R. performed all simulations, collected and analysed all the data and Z.T. wrote the paper.

A Supplementary Information

Here we provide derivations and discussions about the properties of the dynamical system (1-2) and additional supporting figures and text.

Recall from the main text the definitions:

$$V(\mathbf{a}, \mathbf{s}) = \sum_{m=1}^M a_m K_m^2, \quad (4)$$

where

$$K_m = 2^{-k} \prod_{j=1}^N (1 - c_{mj} s_j). \quad (5)$$

Note that in k -SAT there are at most k terms in the product above, hence $0 \leq K_m \leq 1$ for all m . The system of ODEs (1-2) defined in the main document is:

$$\dot{s}_i = \frac{ds_i}{dt} = -\frac{\partial}{\partial s_i} V(\mathbf{a}, \mathbf{s}) = \sum_{m=1}^M 2a_m c_{mi} K_{mi} K_m, \quad i = 1, \dots, N, \quad (6)$$

$$\dot{a}_m = \frac{da_m}{dt} = a_m K_m, \quad m = 1, \dots, M, \quad (7)$$

with $a_m(0) > 0$, $m = 1, \dots, M$ (for example $a_m(0) = 1$), and where

$$K_{mi} = 2^{-k} \prod_{\substack{j=1 \\ j \neq i}}^N (1 - c_{mj} s_j) = \frac{K_m}{1 - c_{mi} s_i}. \quad (8)$$

A. Free variables, solution clusters and attractors. Solution clusters are defined by solutions that can be connected via single-variable flips, always staying within satisfying assignments. For example, consider two k -SAT solutions that differ in exactly one variable, let's say in s_j (at Hamming distance of 1), thus forming a solution cluster of two points in $\mathcal{V}_N = \{-1, 1\}^N$. Then *any* point on the s_j axis in the $[-1, 1]$ *continuous segment* is a fixed-point ($\dot{\mathbf{s}} = \mathbf{0}$, $\dot{\mathbf{a}} = \mathbf{0}$) of the dynamics (6-7), because for the two solutions the value of s_j is irrelevant (called a ‘‘free variable’’), all the clauses being satisfied by the other variables taking values ± 1 . For our dynamical system, the corresponding attractor is an edge of the N -hypercube Q_N , a compact, connected domain/set. It is certainly possible that several solutions in \mathcal{V}_N be connected via single variable flips, with two examples given in Figs. 5a-b. Thus, the *attractors* of the dynamical system (6-7) (or (1) in the main text) in general are compact, connected sets of Q_N spanned by the k -SAT solution clusters and by only those (see also sections D and E). Every point from this attractor set is a fixed-point of the continuous-time (CT) dynamics.

B. Spin variables s remain in $\mathcal{H}_N = [-1, 1]^N$. From Eq. (6):

$$\dot{s}_i = 2 \sum_{m=1}^M a_m c_{mi} (1 - c_{mi} s_i) K_{mi}^2 = 2 \sum_{m=1}^M a_m K_{mi}^2 [(1 - s_i) \delta_{c_{mi}, 1} - (1 + s_i) \delta_{c_{mi}, -1}] \quad (9)$$

This dynamics keeps spins within $[-1, 1]$, because at $s_i = 1$ ($s_i = -1$) we have $\dot{s}_i \leq 0$ ($\dot{s}_i \geq 0$) for any $c_{mi} \in \{-1, 1\}$.

C. Stability of all k -SAT solutions. Domains of attraction. As seen in the main text, all the s points for which $V = 0$, are fixed points of the dynamics (6-7). As shown in Section A, some of these points are not necessarily from \mathcal{V}_N , they can be from the compact domain corresponding to a cluster of solutions from \mathcal{V}_N , when there are free variables. We prove stability by showing that in a vicinity of non-zero volume in \mathcal{H}_N of a k -SAT solution, the function $R \equiv \sum_{i=1}^N s_i^2$ is

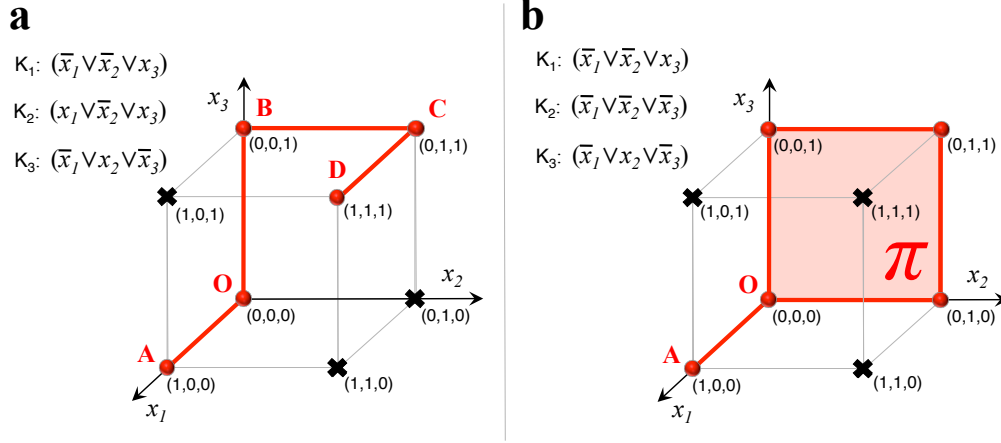


Figure 5: **Example attractors spanned by solution clusters.** Two examples with $k = 3$, $N = 3$, $M = 3$, see the figure for the sets of clauses in each case. In **a** the solution cluster is the set of vertices $\{A, O, B, C, D\}$, while for the dynamical system the corresponding attractor is the *continuous* union of segments $\overline{AO} \cup \overline{OB} \cup \overline{BC} \cup \overline{CD}$ (and the equivalent in the s -space). In **b**, the solution cluster is formed by the four vertices of the shaded square-plate π and vertex A , while for the dynamical system the corresponding attractor is $\pi \cup \overline{AO}$.

monotonically increasing until the dynamics reaches a point in s -space for which $V = 0$ (hence all $K_m = 0$), that is, the trajectory reaches the cluster's domain. From (6):

$$\dot{R} \equiv 2 \sum_{i=1}^N s_i \dot{s}_i = 4 \sum_{m=1}^M a_m K_m \sum_{i=1}^N c_{mi} s_i K_{mi} . \quad (10)$$

Assume that $\mathbf{s}^* \in \mathcal{V}_N$ is a k -SAT solution. Recall that we have k variables in each clause (all the rest have $c_{mi} = 0$). Choosing a clause K_m , let us denote the indices of the variables included as $i = 1, \dots, k$, and order them such that the variables $j = 1, \dots, p$ satisfy the clause, meaning that $(1 - c_{mj} s_j^*) = 0$, and the variables $l = p + 1, \dots, k$ do not satisfy the clause, and thus $(1 - c_{ml} s_l^*) = 2$. Clearly, such a $1 \leq p \leq k$ always exists, since $K_m(\mathbf{s}^*) = 0$. If we are in the corresponding N -dimensional orthant (orthant) of \mathbf{s}^* then $\text{sgn}\{s_i\} = s_i^*$ for all s from this orthant with $0 < |s_i| < 1$. Then $c_{mj} s_j^* = 1$ implies $c_{mj} s_j = |s_j|$ for all $j = 1, \dots, p$ and $c_{ml} s_l^* = -1$ implies $c_{ml} s_l = -|s_l|$ for all $l = p + 1, \dots, k$ in this orthant. Thus:

$$Z_m \equiv \sum_{i=1}^k c_{mi} s_i K_{mi} = K_m \sum_{i=1}^k \frac{c_{mi} s_i}{1 - c_{mi} s_i} = K_m \left(\sum_{j=1}^p \frac{|s_j|}{1 - |s_j|} - \sum_{l=p+1}^k \frac{|s_l|}{1 + |s_l|} \right) \quad (11)$$

Clearly, for any $\sigma > 0$ with $\sigma < \min_j |s_j|$, we have $|s_j|/(1 - |s_j|) > \sigma/(1 - \sigma)$ (for all j) and $|s_l|/(1 + |s_l|) < 1/2$ (since $|s_l| < 1$). Therefore

$$Z_m > K_m \left(\frac{p\sigma}{1 - \sigma} - \frac{k - p}{2} \right) . \quad (12)$$

Hence, if $\sigma > \frac{k-p}{k+p}$, then $Z_m > 0$ (for all m) and from (10) $\dot{R} = \sum_m 4a_m K_m Z_m > 0$, that is

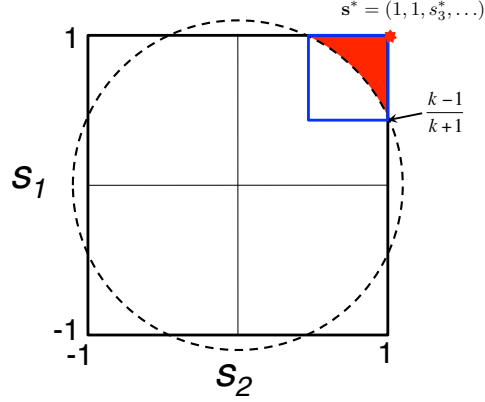


Figure 6: **Domain of attraction, 2D illustration.** If $\mathbf{s}^* \in \mathcal{V}_N$ is a k -SAT solution, and $\text{sgn}(s_i) = s_i^*$, $|s_i| > (k-1)/(k+1)$ are satisfied for all $i = 1, \dots, N$ (inside the blue square) then $dR/dt > 0$. The dynamics cannot leave from inside the domain $\mathcal{C}_N(\mathbf{s}^*)$ (marked with red) as $|s_i| \leq 1$ (see section B). It follows that R grows until it hits the domain of the solution cluster attractor containing \mathbf{s}^* , or \mathbf{s}^* itself, meaning that $\mathcal{C}_N(\mathbf{s}^*)$ is part of the attractor's basin.

the trajectory is strictly increasing its distance from the origin (unless all $K_m = 0$, which means the trajectory is on the attractor, where $\dot{R} = 0$). Since $(k-p)/(k+p)$ is a decreasing function of p , we can choose $p = 1$ and set

$$\sigma = \frac{k-1}{k+1}$$

to define a vicinity of \mathbf{s}^* , with $|s_i| > \sigma$, $i = 1, \dots, N$ within which we are guaranteed $\dot{R} > 0$. Next, consider the corner domain $\mathcal{C}_N(\mathbf{s}^*)$ around \mathbf{s}^* of \mathcal{H}_N cut away by the N -dimensional sphere of radius $\sqrt{N-1 + \sigma^2}$ centered in the origin. See Fig. 6 for an illustration in 2D. Trajectories in all points within this domain have the property $\dot{R} > 0$ or $\dot{R} = 0$, in the latter case the point being on the attractor. For points with $\dot{R} > 0$, the trajectory must necessarily flow towards the boundary part (Q_n) of the hypercube of this domain $\mathcal{C}_N(\mathbf{s}^*)$, away from the surface of the sphere until it hits \mathbf{s}^* , or the attractor of the solution cluster of which \mathbf{s}^* is part of (in case of free variables), lying within $\mathcal{C}_N(\mathbf{s}^*)$. Clearly R cannot increase beyond N , in which case the trajectory is at \mathbf{s}^* .

D. There are no limit cycles in \mathbf{s} . Having a limit cycle in \mathbf{s} which is not a fixed-point means that $s_i(t)$ is a periodic function of t of period $T > 0$, and consequently all its derivatives, including $\dot{s}_i(t)$:

$$s_i(t) = s_i(t + nT), \quad \dot{s}_i(t) = \dot{s}_i(t + nT) \quad (13)$$

for all $i = 1, \dots, N$ and all integers n . Since the K_m are functions of time only through the s_i variables, this implies that all K_m are periodic functions of time as well. From (6) it follows:

$$\dot{s}_i(t + nT) = \sum_{m=1}^M a_m(t + nT) 2c_{mi} K_m(\mathbf{s}(t)) K_{mi}(\mathbf{s}(t)). \quad (14)$$

Formally, the solution for a_m from (7) can be written as

$$a_m(t) = a_m(t_0) \exp \left[\int_{t_0}^t d\tau K_m(\mathbf{s}(\tau)) \right]. \quad (15)$$

Using the periodicity of K_m this leads to $a_m(t + nT) = a_m(t)e^{nI_m}$ with $I_m = \int_0^T K_m(\mathbf{s}(\tau))d\tau$. From (14) and (13) it follows:

$$\sum_{m=1}^M a_m(t) (e^{nI_m} - 1) 2c_{mi}K_m(t)K_{mi}(t) = 0, \quad i = 1, \dots, N \quad (16)$$

which has to hold for any integer n and all times t . Every sum in (16) is of the type

$$\sum_m (x_m^n - 1) f_{mi} = 0, \quad \forall n \in \mathbb{Z}, \quad (17)$$

Where $x_m = e^{I_m}$. Since $K_m \in [0, 1]$ it follows that $I_m \geq 0$ and thus $x_m \geq 1$. Assume that the x_m -s are all different from each other, and consider x_{m^*} to be the largest of them. Then, clearly, increasing n without limit, all other terms in the sum of (17) become arbitrarily small compared to the m^* term and since $x_{m^*} \geq 1$, this forces $f_{m^*i} = 0$. Thus the m^* term must be absent from the sum (17), and we can repeat the procedure with the next largest x_m term leading to $f_{mi} = 0$, etc. Hence, all $f_{mi} = 0$ and thus $\dot{s}_i = \sum_m f_{mi} = 0$. If the x_m -s are equal ‘‘in blocks’’, with a similar procedure we can show that for every block b we must have $(x_b^n - 1) \sum_{m \in b} f_{mi} = 0$, for all n . This implies that either $x_b = 1$, or $\sum_{m \in b} f_{mi} = 0$. In the former case we thus must have for all $m \in b$, $I_m = 0$ and hence $K_m = 0$ (recall, that $K_m \geq 0$) which actually implies that the corresponding $f_{mi} = 0$, since $f_{mi} \propto K_m$. Hence, either way, $\sum_{m \in b} f_{mi} = 0$ for all blocks, and therefore, again, $\dot{s}_i = \sum_m f_{mi} = 0$ meaning that we are in a fixed point, contradicting our original assumption.

E. Fixed-points and attractors in \mathcal{H}_N . We have seen that the dynamics in Ω admits fixed point solutions ($\dot{\mathbf{s}} = \mathbf{0}$, $\dot{\mathbf{a}} = \mathbf{0}$) only on the boundary Q_N , either as isolated points from \mathcal{V}_N (k -SAT solutions), or in form of compact, connected domains (if there are free variables) corresponding to k -SAT solution *clusters*. This holds because $\dot{\mathbf{a}} = \mathbf{0}$ if and only if $K_m = 0$ for all m , which is possible (due to their product form, (5)) only if some of the spins are ± 1 , hence they form k -SAT solutions. The question is whether there are other *stable* fixed points *within* \mathcal{H}_N (thus in \mathbf{s} -space), but with not all $K_m = 0$, in which the dynamics could get stuck indefinitely. In principle it could happen that there are points $\mathbf{s} \in \mathcal{H}_N$ for which $\dot{\mathbf{s}} = \mathbf{0}$ but the dynamics (7) of the auxiliary variables is not able to unstuck the spin variables from there. The answer is negative that is, there are no such *stable* fixed points and here we sketch its proof. However, as we will see, there can be unstable fixed-points, which play an important role in the dynamics within \mathcal{H}_N . In subsection E.1 below we discuss how the trajectory must leave any domain \mathcal{D} within \mathcal{H}_N that does not have a solution in it.

Let us assume that the dynamics at time \bar{t} arrives into a point $\bar{\mathbf{s}} = \mathbf{s}(\bar{t}) \in \mathcal{H}_N$ for which:

$$\dot{s}_i(\bar{t}) = - \left. \frac{\partial}{\partial s_i} V(\mathbf{a}, \mathbf{s}) \right|_{\bar{s}_i} = 2 \sum_{m=1}^M a_m(\bar{t}) c_{mi} K_m(\bar{\mathbf{s}}) K_{mi}(\bar{\mathbf{s}}) = 0, \quad i = 1, \dots, N, \quad (18)$$

and not all K_m -s are zero. Let us denote $\bar{a}_m \equiv a_m(\bar{t})$, $\bar{K}_m \equiv K_m(\bar{s})$. Then, using (8), system (18) can be thought of as a homogeneous system of equations for the \bar{a}_m variables:

$$\sum_{m=1}^M \bar{a}_m \bar{K}_m^2 \frac{c_{mi}}{1 - c_{mi} \bar{s}_i} = \sum_{m=1}^M \bar{a}_m \bar{u}_{mi} = 0, \quad i = 1, \dots, N. \quad (19)$$

As there are more clauses than variables ($M > N$), system (19) in general defines an $M - r$ -dimensional domain in \mathbf{a} -space, namely, the *left null-space* $\ker(\mathbf{U}^\top)$ of the $M \times N$ matrix $\mathbf{U} = \{u_{mi}\}$ of rank $r \leq N$. Since not all K_m -s are zero, the a_m variables will change over time, according to (7). In order for the dynamics to be stuck in \bar{s} indefinitely, one must have condition (19) hold for *all later times* $\bar{t} + \tau$. Using $a_m(t) = \bar{a}_m e^{\int_{\bar{t}}^{t+\tau} dt \bar{K}_m} = \bar{a}_m e^{\tau \bar{K}_m}$, the condition becomes:

$$\sum_{m=1}^M e^{\tau \bar{K}_m} \bar{a}_m \bar{u}_{mi} = 0, \quad i = 1, \dots, N, \quad \text{for all } \tau \geq 0. \quad (20)$$

If there is a *single* m^* for which $\bar{K}_{m^*} > \bar{K}_m$ for all m , then clearly, the lhs of (20) becomes dominated by this maximum exponential term and (20) becomes violated, and hence the dynamics becomes unstuck from \mathbf{s} . The only way that (20) has a chance to hold for arbitrary τ , if the K_m -s are equal in blocks of at least size two (since $\bar{u}_{mi} \propto c_{mi} \in \{-1, 0, 1\}$, cancellations are possible). That means that there are at least $M/2$ equations expressing the equalities of the corresponding K_m -s. Since there are N spin variables and we are looking at $\alpha = M/N > 2$ (no point solving SAT in the very easy phase) there are more (nonlinear) equations than variables and thus it drastically reduces the chances of finding an \bar{s} solution satisfying these. Assuming that such \bar{s} exists (one cannot exclude it in general), we need to analyze this case, in particular whether the equality in blocks of the K_m -s is an “attractive” condition by the dynamics for some \bar{s} . In other words, we need a stability analysis of \bar{s} . It is important to note that \bar{s} is not a standard fixed point in the traditional sense. Since the dynamics is also driven by the auxiliary variables, we have the continuous domain of the left null-space $\ker(\mathbf{U}^\top)$ as “fixed point” for the dynamics. As soon as the a_m variables leave this domain, the dynamics gets unstuck from \bar{s} , and only then. For this reason, the linear stability analysis around \bar{s} is somewhat different from a standard stability analysis.

Thus, let us assume that (20) holds for arbitrary τ for some \bar{s} . Since the dynamics is in the (\mathbf{s}, \mathbf{a}) -space, let us consider a small deviation ϵ such that $\mathbf{a} = \bar{\mathbf{a}} + \epsilon$, $\epsilon_m \geq 0$, $m = 1, \dots, M$, $|\epsilon| \ll 1$, at $\tau = 0$. Clearly, one can easily choose the ϵ_m variables, such that

$$\sum_{m=1}^M \epsilon_m \bar{u}_{mi} \neq 0, \quad i = 1, \dots, N, \quad (21)$$

that is, ϵ is any vector that is not from the left null-space of the $\{\bar{u}_{mi}\}$ matrix. For example, if $\bar{u}_{11} \neq 0$, then $\epsilon = (\epsilon |\bar{u}_{11}|, 0, \dots, 0)$, $\epsilon > 0$, $\epsilon \ll 1$ would suffice. From (18) it then follows, that the s_i variables start changing, as $\dot{s}_i = 2 \sum_m \epsilon_m \bar{u}_{mi} \neq 0$. Recall that in k -SAT we are only considering problems in which every variable is present in both its direct and negated forms, in different clauses. If this wasn't the case, that is, if a variable s_i when present in a clause would be

only present in its direct form (no negated form anywhere), then we could easily set the value of that variable to +1 and automatically satisfy all the clauses in which it is present and reduce the problem to a smaller one. Additionally, if all c_{mi} -s would have the same sign, one could never have (19) satisfied in the first place, since $\bar{a}_m > 0$ and $1 - c_{mi}\bar{s}_i > 0$. This means, that for any $\bar{s}_i \neq 0$, there will be clauses for which the K_m -s will increase and others for which it will decrease. Since these variations are continuous, the ϵ shift vector can always be chosen such that there will appear a single largest clause K_{m^*} , resulting in the case already discussed above, with \mathbf{a} leaving exponentially fast the left null-space $\ker(\mathbf{U}^\top)$ showing that the dynamics is unstable in $\bar{\mathbf{s}}$.

Clearly, it is in general mathematically possible for the K_m -s to be equal in blocks such that (20) holds for all τ , defining regions of zero (Lebesgue) measure in \mathcal{H}_N . As we have just shown, these fixed regions or “points”, however, are all unstable for the dynamics. The linearized neighborhoods of these points are characterized by the stable and unstable subspaces spanned by the eigenvectors with contracting and expanding eigenvalues, respectively [31]. For this reason, these type of fixed points are called hyperbolic fixed points or saddles. Moving away from the linearized neighborhoods, these two subspaces form the stable and unstable manifolds of the saddle, which then extend endlessly into the phase space. While two stable and two unstable manifolds can never cross, the stable and unstable manifolds can intersect, forming either homoclinic intersections (when the two manifolds belong to the same saddle) or heteroclinic intersections (they come from two different saddles), see Ref [31]. Chaotic dynamics appears as the result of homoclinic or heteroclinic intersections.

E.1 Escape from an arbitrary domain. So far we have shown an important property, that is, the dynamics cannot be captured by a non-solution *fixed point* (for any formula). We have also shown in Section D that it cannot be captured by a limit cycle either. The question remains, however, whether it could be captured by some other type of non-solution attractor, possibly even a chaotic attractor. One way to show that this cannot happen, is to prove that the trajectory cannot stay confined for arbitrarily long times within an *arbitrary domain* \mathcal{D} in the s -space ($\mathcal{D} \subset \mathcal{H}_N$) that *does not contain a solution*. The following description is a brief sketch for what happens during the dynamics, and it forms the elements of a proof (to be published elsewhere).

Let us assume that at some point in time t_0 , the trajectory is in \mathcal{D} , $\mathbf{s}(t_0) \in \mathcal{D}$. After eliminating the auxiliary variables from (6) using their expression from (15), the rate of change for the spin variables becomes:

$$\frac{ds_i}{dt} = \sum_{m=1}^M 2a_m(t_0)c_{mi}K_{mi}K_m e^{\int_{t_0}^t d\tau K_m(\mathbf{s}(\tau))}. \quad (22)$$

As \mathbf{s} is confined to \mathcal{D} , there is always a subset of constraints (K_m -s) that are bounded away from zero within \mathcal{D} (otherwise we are in a solution, which contradicts the assumption that \mathcal{D} has no solutions in it). After long enough times, the exponentials in (22) involving these constraints grow very large, and unless they balance each other perfectly (due to the c_{mi} -s) in every \mathbf{s} point along the trajectory in \mathcal{D} , one of them will overtake the others and overgrow them ($\exp\left[\int_{t_0}^t d\tau K_m\right] > e^{K(t-t_0)}$), at least for a while. In this time interval the sign for some of the ds_i/dt -s will stabilize into either just positive or just negative and their magnitude will grow *expo-*

nentially fast ($|Ae^{at} - Be^{bt}| \sim e^{\max\{a,b\}t}$). When that happens, at large enough t , the trajectory will outburst from \mathcal{D} (a finite domain). It can also happen, however, that the constraints oscillate around each other, and hence their role as to which one is the leading one in (22), changes over time. This can result in an oscillatory behavior in the corresponding ds_i/dt -s and of the trajectory. However, even in this case, all terms corresponding to the constraints are growing exponentially fast, and the differences between the growing exponentials have increasingly wilder fluctuations, which eventually leads to the outburst of the trajectory from \mathcal{D} . One can show that any situation in which the exponential terms corresponding to the constraints in all the N equations perfectly cancel each other (so that there is no leading exponential) will be unstable against small perturbations, similarly to the case of a fixed point.

F. Finite Size Lyapunov Exponents (FSLE). We have employed the FSLE method [32] from nonlinear dynamics theory to provide a distributed measure of chaos in our system. The FSLE describes the local average strength of exponential separation of trajectories and it has been extensively used to analyze turbulent flows and processes, including in the atmosphere [33] and oceans [34]. The FSLE in a point s is given by $\phi(s, \varepsilon_0, \varepsilon) = \langle \tau^{-1} \ln \varepsilon / \varepsilon_0 \rangle$, where $\varepsilon_0 = |s - s'|$ is a small initial separation of two points with s' chosen in a random direction, and τ is the time needed for the separation of the corresponding trajectories started from these two points to reach the given separation ε . The average $\langle \cdot \rangle$ is over the random directions of s' . In Fig 7 $\varepsilon = 30\varepsilon_0$ and ϕ is averaged for 50 different randomly oriented initial separations.

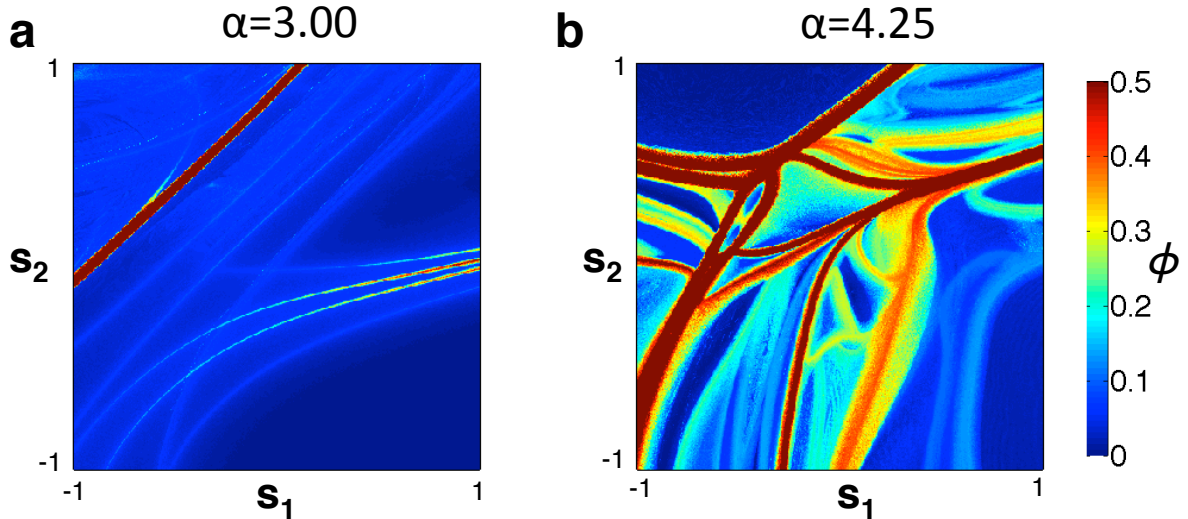


Figure 7: **Finite-Size Lyapunov Exponents.** The colour maps show Finite Size Lyapunov Exponents ϕ measured on a problem with $k = 3$, $N = 50$ at **a**: $\alpha = 3$ and **b**: $\alpha = 4.25$. Initially, all s_j have a random, but fixed value except s_1 and s_2 which are varied along a 400×400 grid. FSLE values are coded with colors, shown by the color bar. Enhanced chaotic behavior appears for hard formulae.

G. Random k -XORSAT. In k -XORSAT there are given M parity check equations (constraints) [35, 36, 37], each involving k specified Boolean variables and a parity bit $y_m = \{0, 1\}$:

$$x_{i_1}^m + \dots + x_{i_k}^m \equiv y_m \pmod{2}, \quad m = 1, \dots, M. \quad (23)$$

The k distinct variables present in a parity check equation are chosen uniformly at random from the set of x_1, \dots, x_N variables. The goal is to assign Boolean, $\{0, 1\}$ values to the variables such that all parity checks are satisfied. As shown in propositional calculus, any propositional formula can be transformed into its conjugate normal form (CNF), and hence boolean decision problems can all be cast into a k -SAT problem. Once k -XORSAT is transformed into k -CNF (Conjugate Normal Form), it becomes a k -SAT problem over a specific ensemble of clauses, hence our dynamical system (1) can be used to solve k -XORSAT (or any boolean decision problem). For $k = 3$ we use four 3-SAT clauses to encode one parity check equation.

Random XORSAT also goes through phase transitions [36, 37] when increasing the constraint density $\gamma = M/N$. The dynamical phase transition takes place at γ_d (for 3-XORSAT $\gamma_d = 0.8185$), when the unique solution cluster existing at $\gamma < \gamma_d$ breaks into an exponentially large number of clusters. The second phase transition is the SAT/UNSAT transition at $\gamma_c > \gamma_d$, with $\gamma_c = 0.9179$ for 3-XORSAT [37]. Constraint satisfaction formulae can be represented as hypergraphs with nodes representing the variables and with hyperlinks representing the constraints connecting the variables present in them. To find the various transitions for k -XORSAT, however, it is actually better not to bring it into CNF form (we do that for simulations with our system (6),(7)). Using this representation, it was proven [37] that γ_d corresponds to the constraint density where the hyperloops (in this non-CNF form hypergraph) appear with non-zero statistical weight in the limit of $N \rightarrow \infty$. As chaotic behavior in our dynamical system (1) appears already at one of the smallest (finite) hyperloop motifs, it therefore also appears at exactly the same γ_d that Mézard et.al. calculated [37]. Fig 8e) shows the full hypergraph for a small specific instance of 3-XORSAT without a *core* at $\gamma = 9/14 = 0.64$ (after performing the leaf-removal algorithm described in [37] the remaining hyperloops form the core of the XORSAT instance). As the graph in Fig 8e) has no core (no hyperloops), the corresponding basin boundary is indeed smooth, i.e., there is no (transient) chaos, also illustrated in Fig 8a). However, once we add more constraints (for example the specific ones shown in Fig 8f)), giving $\gamma = 12/14 = 0.85$ the core appears (shown in red in Fig 8f)), and the basin boundaries become fractal, see Fig 8b)-d).

H. Polynomial continuous-time complexity for a fixed number of formulae. We now show that Eq (2) of the main text implies the stronger result of having polynomial continuous - time complexity even for leaving a *fixed number* (not fraction!) of formulae unsolved in the limit $N \rightarrow \infty$. For a given N and $M = \alpha N$ there are a total of

$$\Theta_\alpha^{(k)}(N) = \binom{2^k \binom{N}{k}}{\alpha N}$$

k -SAT formulae. If c is a small integer constant (independent of N), setting $p = c/\Theta_\alpha^{(k)}(N)$ in (2) of the main text yields

$$t(p, N) = b^{-1} N^\beta \left[\ln(r/c) + \ln \Theta_\alpha^{(k)}(N) \right].$$

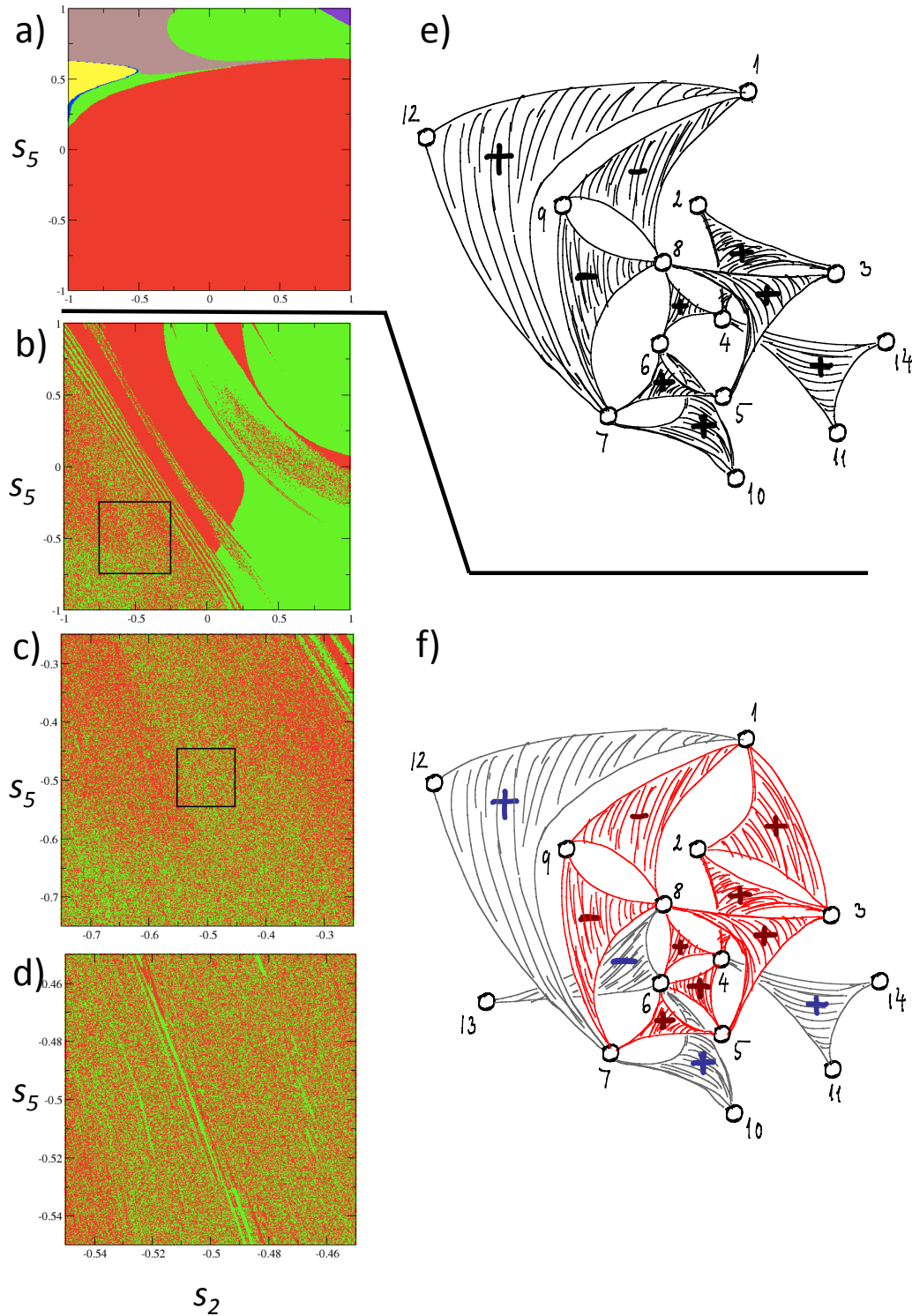


Figure 8: **3-XORSAT**. a) basins of attraction to solutions for a formula given by the hypergraph in e), which has no hyperloops (core). b) basins of attraction to solutions for the formula in f), which has a core (shown in red). c) is the magnification of the small black rectangle from b), and d) is a magnification of a small black rectangle from c). In the hypergraphs e) and f) the “triangles” represent hyperedges/parity checks ($k = 3$) and the signs correspond to y_j -s.

However, for fixed α , $\ln \Theta_\alpha^{(k)}(N) = \alpha(k-1)N \ln N + \mathcal{O}(\ln N)$ as $N \rightarrow \infty$, which implies that

$$t(p, N) \sim N^{\beta+1} \ln N,$$

i.e., still showing polynomial CT complexity. Thus, assuming that (2) holds for all N , the fact that only a constant number of problems may not be solved in polynomial time for $N \rightarrow \infty$ indicates that the algorithm runs in polynomial continuous-time on *almost all* hard k -SAT instances (the probability to find an instance not solvable in polynomial time by this solver is zero in the $N \rightarrow \infty$ limit).

I. Computational complexity in the number of discrete steps. Since the numerical integration happens on a Turing machine, the true continuous trajectory is being approximated by the Runge-Kutta (RK) algorithm [38] with sufficiently many discrete points, lying close to it, within a tube of preset diameter ε (see Fig. 9). When we monitor the fraction of formulae left unsolved p as function of the *number of discretization steps* n_{step} taken by the algorithm for hard SAT formulae (from the frozen phase), we find that $p(n_{step})$ has a *power-law* decay, well approximated by $p(n_{step}) = u(v + n_{step})^{-\eta}$, see Fig. 10a. The exponent η also has a power-law N -dependence (see Fig. 10b): $\eta(N) = dN^{-\delta}$ with $\delta \simeq 1.09 \simeq 1$ (the N -dependence of u and v are weak). This implies an *exponential behavior* for the number of time steps $n_{step}(p, N)$ needed to miss solving only a p -th fraction of the formulae:

$$n_{step}(p, N) = e^{N^{\delta} \frac{1}{d} \ln \frac{u}{p}} - v, \quad (24)$$

showing exponential time-complexity for the discretized algorithm ran by a digital computer (Turing machine). For easy formulae, however, (such as those drawn at random for $\alpha = 3$), $p(n_{step})$ has an exponential decay, just as $p(t)$, implying polynomial complexity for the discretized algorithm as well, see the inset of Fig 10a.

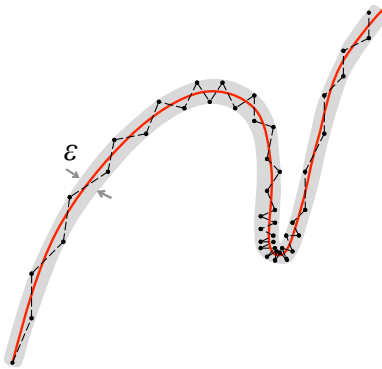


Figure 9: **Approximating the continuous-time trajectory.** The RK algorithm must compute a large number of discrete points in high curvature regions in order to stay within a prescribed precision ε .

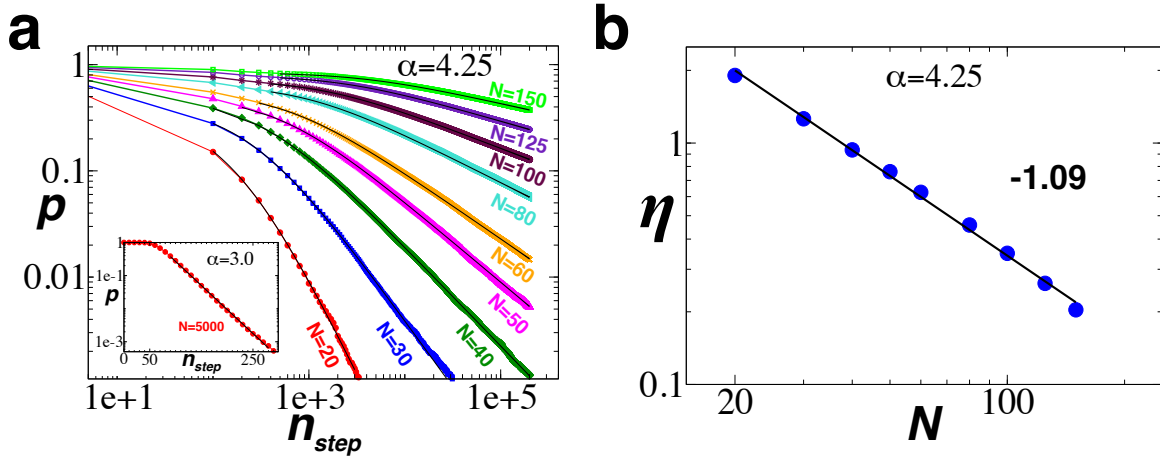


Figure 10: **Discrete time complexity.** **a:** Fraction of problems $p(n_{step})$ left unsolved after n_{step} discretization steps, at $\alpha = 4.25$, $k = 3$ for different system sizes $N = 20, 30, 40, 50, 60, 80, 100, 125, 150$ (different colors). Averages were done over 10^5 instances for each N , except for $N = 150$ where 3×10^4 instances were used. The black continuous lines are $p(n_{step}) = u(v + n_{step})^{-\eta}$. The inset (log-lin plot) shows $p(n_{step})$ from 10^5 instances with $N = 5000$ at $\alpha = 3$. In this easy-SAT region $p(n_{step})$ shows a similar exponential decay as $p(t)$ shown in Fig3a, main text. **b:** The exponent η follows: $\eta(N) = dN^{-\delta}$, $\delta \simeq 1.09$.

J. Dependence on discretization error. The continuous-time variable t and the decay of p as function of t is only weakly dependent on the discretization error ε by the RK solver, with a slight shift towards even cleaner exponentials when lowering ε , see Fig. 11a.

As stated in the main text, the polynomial CT complexity is not the consequence of a log-transformation on the time variable t . The scaling of the *length* L of the continuous-time trajectory measured from the initial point until it finds a solution also scales polynomially with N . However, this measure is more sensitively affected by the discretization error ε . This is because, as illustrated in Fig. 9, the length computed as the sum of the lengths of the straight segments between discretization steps *overestimates* the analog trajectory length (continuous red line). Fig. 11b shows the fraction of formulae p left unsolved by trajectories of length not longer than L (measured in \mathcal{H}_N), as function of L for different discretization errors ε . The convergence to clean exponentials is evident as ε is lowered.

K. Analogy with fluid turbulence Continuous-time processes are common in nature, from fluid flows to information processing in the brain; even our perception of time is arguably of analog nature. While transient chaos can appear in many dynamical systems, long chaotic transients typically occur in a parameter region preceding the permanently chaotic regime. If the average lifetime of transients in a dynamical system depends on an extensive parameter of the system, supertransients (or superpersistent chaotic transients) may appear [39, 40]. The only experiments confirming the existence of such supertransients are those done in long-pipe flow experiments.

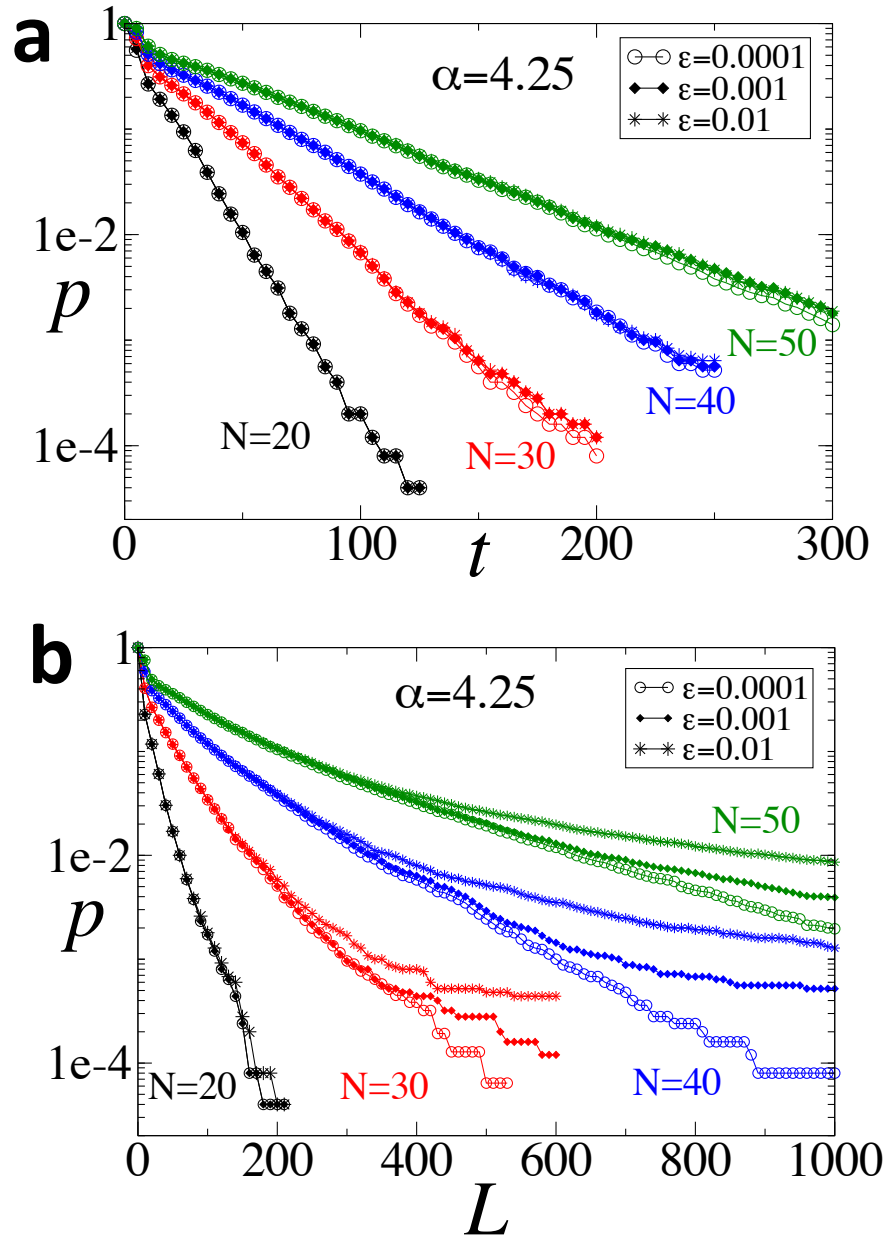


Figure 11: **Sensitivity to discretization error.** **a:** Fraction of problems $p(t)$ left unsolved by continuous-time t , at $\alpha = 4.25$, $k = 3$ for system sizes $N = 20, 30, 40, 50$ (different colors) and for different error parameters of the adaptive Runge-Kutta method [38]: $\epsilon = 0.0001, 0.001, 0.01$. Here ϵ is the maximal relative error allowed during the RK integration. Statistics was done on 2.5×10^4 instances for each N . **b:** The fraction of problems $p(L)$ left unsolved by trajectories of length at most L (measured in \mathcal{H}_N), for the same problems as in **a**.

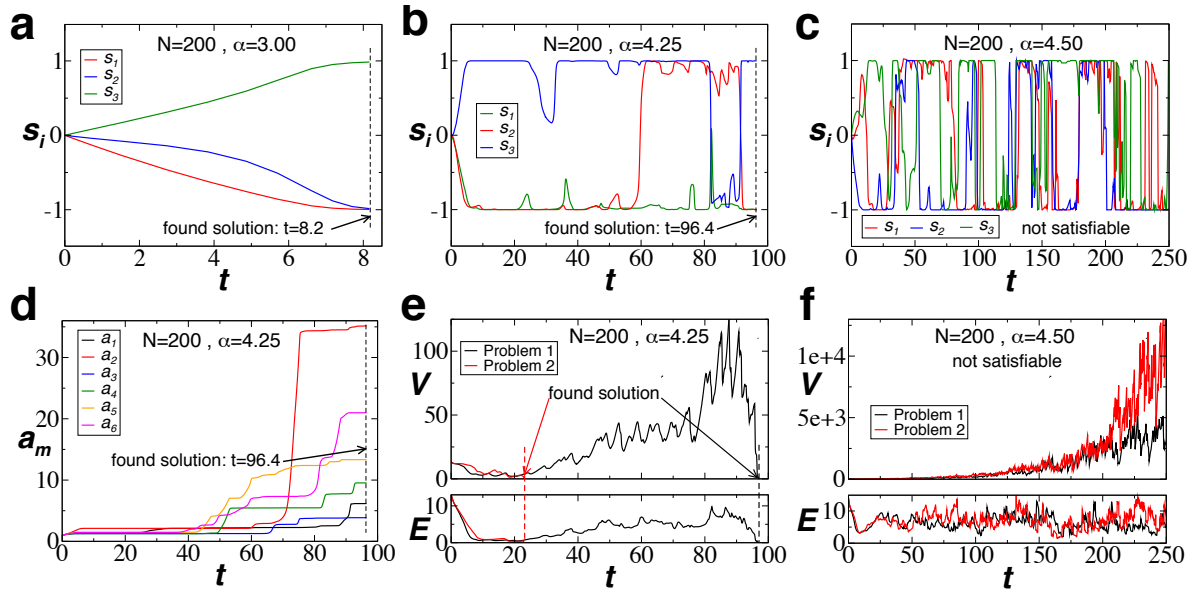


Figure 12: **Time evolution of variables and energy functions.** Time evolution of three variables $s_i(t)$ (different colors) for a formula with $k = 3$, $N = 200$ and **a:** $\alpha = 3$, characterized by rapid and straightforward convergence; in **b:** at $\alpha = 4.25$, presenting much longer, and chaotic trajectories, and **c:** for an unsatisfiable formula at $\alpha = 4.5$. **d:** Time series of six different auxiliary variables $a_m(t)$ shown with different colors for the same problem as in **b**. Time series of $E(\mathbf{s})$ and $V(\mathbf{s}, \mathbf{a})$ as function of the continuous time t , for two different problems (red and black) with $k = 3$, $N = 200$ at **e:** $\alpha = 4.25$ and **f:** for two unsatisfiable formulae at $\alpha = 4.5$.

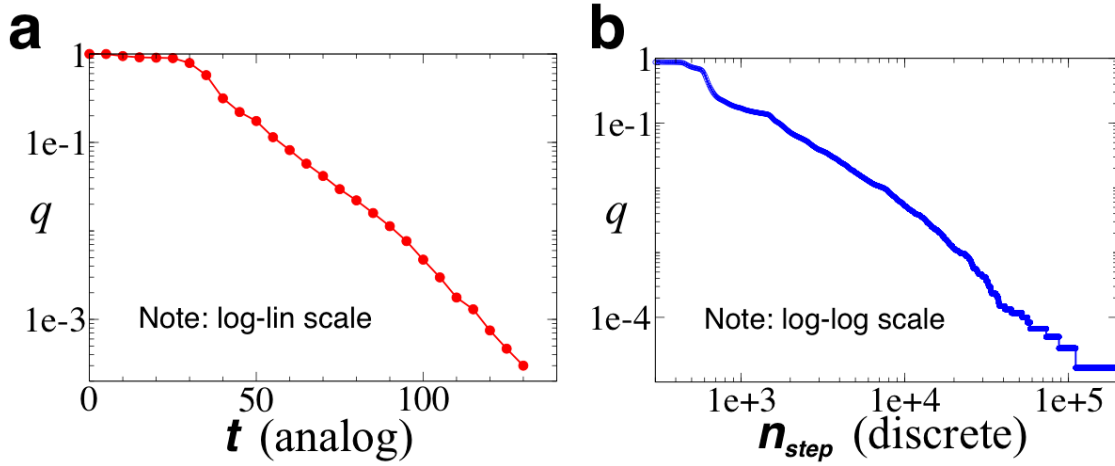


Figure 13: **Exponential decay for a single instance.** For single 3-SAT instance with $N = 40$, at $\alpha = 4.25$ we start the dynamics from 60000 different random initial conditions. **a:** Similarly to Fig 3a of the main text the fraction of trajectories $q(t)$, which did not find the solution by analog-time t shows an exponential decay as function of t . **b:** The fraction of trajectories, $q(n_{step})$ still searching for the solution after n_{step} discretization steps, however, shows a power-law behavior.

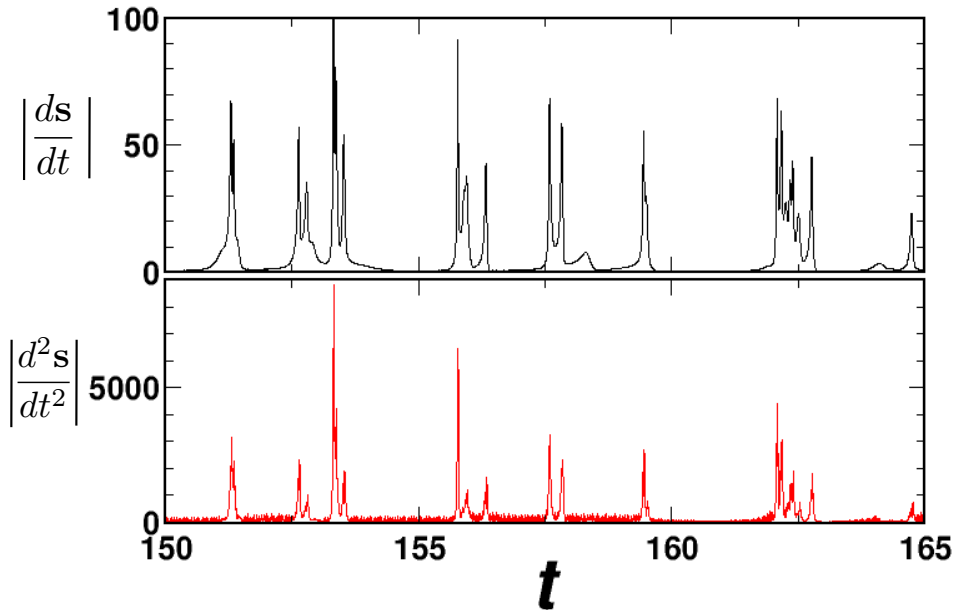


Figure 14: **Intermittent behaviour.** **a:** The velocity $\left| \frac{ds}{dt} \right|$ and the acceleration $\left| \frac{d^2s}{dt^2} \right|$ along the trajectories in the hard-SAT phase ($N = 100$, $\alpha = 4.25$, 3-SAT) show intermittency as function of time similar to turbulent flows [43]. **b:** Same as (a) on log-linear scale.

Here, turbulent/chaotic behavior appears before the flow enters its laminar phase (parabolic velocity profile), which is its only asymptotic attractor [41, 42]. One can think of fluid turbulence in this case as nature's search for equilibrium, practically solving a hard global optimization problem. Fig 14 perhaps takes this analogy further: it shows the fluctuations of the instantaneous velocity and acceleration for a typical trajectory for a hard formula from the frozen region as function of time, revealing intermittent behavior, typically found in turbulence, see Fig 1 of the paper by Meneveau and Sreenivasan [43].

References

- [1] Cook, S. The complexity of theorem-proving procedures. *ACM Symp. on Theory of Comp.* 151-158 (1971).
- [2] Fortnow, L. The status of the P versus NP problem. *Commun. ACM* 52, 78-86 (2009).
- [3] Garey, M. R. , Johnson, D. S. *Computers and Intractability; A Guide to the Theory of NP-Completeness* (W. H. Freeman , Co., New York, NY, USA, 1990).
- [4] Kadanoff, L.P. , Tang, C. Escape from strange repellers. *PNAS* 81, 1276-1279 (1984).
- [5] Tél, T. , Lai, Y.-C. Chaotic transients in spatially extended systems. *Physics Reports* 460, 245-275 (2008).
- [6] Lai, Y.-C. , Tél, T. *Transient Chaos: Complex Dynamics on Finite-Time Scales* (Springer 2011).
- [7] Ott, E. *Chaos in dynamical systems.* (2nd edition, Cambridge Univ. Press, 2002).
- [8] Nusse, H.E. , Yorke, J.A. Basins of attraction. *Science* 271, 1376-1380 (1996).
- [9] Grebogi, C., Ott, E. , Yorke, J.A. Basin boundary metamorphoses: changes in accessible boundary orbits. *Physica D* 24, 243-262 (1987).
- [10] Elser, V., Rankenburg, I. , Thibault, P. Searching with iterated maps. *PNAS* 104, 418-423 (2007).
- [11] Achlioptas, D. , Ricci-Tersenghi, F. Random formulae have frozen variables. *SIAM J. Comput.* 39, 260-280 (2009).
- [12] Zdeborová, L. , Mézard M. Locked constraint satisfaction problems. *Phys. Rev. Lett.* 101, 078702 (2008).
- [13] Cvitanović, P., Artuso, R., Mainieri, R. Tanner, G. , Vattay, G. *Chaos: Classical and Quantum*, ChaosBook.org/version13 (Niels Bohr Institute, Copenhagen 2010)
- [14] Branicky, M. Analog computation with continuous ODEs. *IEEE Workshop on Physics and Computation* (Dallas, TX, 1994), pp. 265 274.
- [15] Siegelmann, H. T. Computation beyond the Turing limit. *Science* 268, 545-548 (1995).
- [16] Moore, C. Recursion theory on the reals and continuous-time computation. *Theor. Comp. Science*, 162, 23-44 (1996).
- [17] Liu, S.-C., Kramer, J., Indiveri, G., Delbruck, T. , Douglas, R. *Analog VLSI: Circuits and Principles* (MIT Press, Cambridge, MA, 2002).

- [18] Chua, L.O. , Roska, T. Cellular Neural Networks and Visual Computing: Foundations and Applications (Cambridge University Press, NY, USA, 2005).
- [19] Gu, J., Gu, Q. , Du, D. On optimizing the satisfiability (SAT) problem. *J. of Comp. Sci. and Techn.* 14, 1-17 (1999).
- [20] Nagamatu, M. , Yanaru, T. On the stability of Lagrange programming networks for satisfiability problems of propositional calculus. *Neurocomputing* 13, 119-133 (1996).
- [21] Wah, B. W. , Chang, Y.-J. Trace-based methods for solving nonlinear global optimization and satisfiability problems. *J. Glob. Opt.* 10, 107-141 (1997).
- [22] Achlioptas, D., Coja-Oghlan, A. , Ricci-Tersenghi, F. On the solution-space geometry of constraint satisfaction problems. *Random Struct. Alg.* 38, 251-268 (2011).
- [23] Molloy, M. Cores in random hypergraphs and Boolean formulae. *Random Struct. Alg.* 27, 124-135 (2005).
- [24] Mézard, M., Ricci-Tersenghi, F. , Zecchina, R. Two solutions to diluted p-spin models and XORSAT problems. *J. Stat. Phys.* 111, 505-533 (2003).
- [25] Mézard, M., Parisi, G. , Zecchina, R. Analytic and algorithmic solution of random satisfiability problems. *Science* 297, 812-815 (2002).
- [26] Achlioptas, D., Naor, A. , Peres, Y. Rigorous location of phase transitions in hard optimization problems. *Nature* 435, 759-764 (2005).
- [27] Mertens, S. Mézard, M., Zecchina, R. Threshold values of random k-SAT from the cavity method. *Rand. Struct. Alg.*, 28, 340-373 (2006).
- [28] Parisi, G. Some remarks on the survey decimation algorithm for k-satisfiability. *arXiv:cs/0301015* (2003).
- [29] Seitz, S., Alava, M., and Orponen, P. Focused local search for random 3-satisfiability. *J. Stat. Mech.*, P06006 (2005).
- [30] Hof, B., de Lozar, A., Kuik, D.J., Westerweel, J. Repeller or Attractor? Selecting the dynamical model for the onset of turbulence in pipe flow. *Phys. Rev. Lett.* 101, 214501 (2008).
- [31] E. Ott. *Chaos in Dynamical Systems*. Cambridge UP, (2000).
- [32] Aurell, E., Boffetta, G., Crisanti, A., Paladin, G. Vulpiani, A. Predictability in the large: an extension of the concept of Lyapunov exponent. *J. Phys. A* **30**, 1 (1997).
- [33] Koh, T.-Y. Legras, B. Hyperbolic lines and the stratospheric vortex. *Chaos* **12**, 382 (2002).
- [34] Ovidio, F.d, Fernández, V., Hernández-García, E. Lopez, C. Mixing structures in the Mediterranean Sea from finite-size Lyapunov exponents. *Geophys. Res. Lett.* **31**, L17203 (2004).

- [35] T.J. Schaefer. In *Proc. 10th STOC, ACM, San Diego, CA, USA*, pp 216
- [36] N. Creignou, H. Daudé and O. Dubois. *Comb. Prob. Comp.* **12**, 113 (2003).
- [37] M. Mézard, F. Ricci-Tersenghi and R. Zecchina. Two solutions to diluted p -spin models and XORSAT problems. *J. Stat. Phys.* **111** 505 (2003).
- [38] Press, W., Teukolsky, S., Vetterling, W. Flannery, B. *Numerical Recipes 3rd Edition: The Art of Scientific Computing* (Cambridge University Press, NY, USA,2007).
- [39] T. Tel, Y.-C. Lai, *Physics Reports* **460**, 245 (2008). (Springer 2011).
- [40] Y.-C. Lai, T. Tel *Transient Chaos: Complex Dynamics on Finite-Time Scales* (Springer 2011).
- [41] B. Hof, J. Westerweel, T. Schneider, B. Eckhardt, Finite lifetime of turbulence in shear flows, *Nature* **443**, 59 (2006)
- [42] B. Hof, A. de Lozar, D.J. Kuik and J. Westerweel, Repeller or attractor? Selecting the dynamical model for the onset of turbulence in pipe flow, *Physical Review Letters*, **101**, 214501 (2008)
- [43] C. Meneveau, K.R. Sreenivasan, The multifractal nature of turbulent energy dissipation. *J. Fluid. Mech.* **224**, 429 (1991).